Characterization of the range effect in synthetic aperture radar images of concrete specimens for width estimation

Ahmed Alzeyadi, Tzuyang Yu

Ahmed Alzeyadi, Tzuyang Yu, "Characterization of the range effect in synthetic aperture radar images of concrete specimens for width estimation," Proc. SPIE 10599, Nondestructive Characterization and Monitoring of Advanced Materials, Aerospace, Civil Infrastructure, and Transportation XII, 1059916 (27 March 2018); doi: 10.1117/12.2294540

SPIE.

Event: SPIE Smart Structures and Materials + Nondestructive Evaluation and Health Monitoring, 2018, Denver, Colorado, United States

Characterization of the Range Effect in Synthetic Aperture Radar Images of Concrete Specimens for Width Estimation

Ahmed Alzeyadi and Tzuyang Yu

Department of Civil and Environmental Engineering
University of Massachusetts Lowell
One University Avenue, Lowell, MA 01854, U.S.A.

ABSTRACT

Nondestructive evaluation (NDE) is an indispensable approach for the sustainability of critical civil infrastructure systems such as bridges and buildings. Recently, microwave/radar sensors are widely used for assessing the condition of concrete structures. Among existing imaging techniques in microwave/radar sensors, synthetic aperture radar (SAR) imaging enables researchers to conduct surface and subsurface inspection of concrete structures in the range-cross-range representation of SAR images. The objective of this paper is to investigate the range effect of concrete specimens in SAR images at various ranges (15 cm, 50 cm, 75 cm, 100 cm, and 200 cm). One concrete panel specimen (water-to-cement ratio = 0.45) of 30-cm-by-30-cm-by-5-cm was manufactured and scanned by a 10 GHz SAR imaging radar sensor inside an anechoic chamber. Scatterers in SAR images representing two corners of the concrete panel were used to estimate the width of the panel. It was found that the range-dependent pattern of corner scatters can be used to predict the width of concrete panels. Also, the maximum SAR amplitude decreases when the range increases. An empirical model was also proposed for width estimation of concrete panels.

Keywords: concrete, synthetic aperture radar, width estimation, microwave

1. INTRODUCTION

Portland cement concrete is the most widely used construction material around the world. One way to evaluate the condition of concrete structures is nondestructive evaluation (NDE). Existing NDE methods include visual inspection, acoustic/ultrasonic testing, thermo infrared, radiography, and microwave/radar sensors. Synthetic aperture radar (SAR) imaging is relatively a new method among microwave/radar sensors in civil engineering. SAR imaging is capable of assessing the surface and subsurface regions of concrete structures such as bridges and buildings. In SAR imaging system, a two directional (2D) range and cross-range (r, r_x) plane is defined. Range (r) is the line sight direction between the radar and the target. Cross-range (r_x) is the travelling direction of radar system in horizontal direction. Changing the range of a SAR imaging system can affect the resolution of the SAR images for surface sensing. In SAR imaging system, the target size is also important because it determines the image resolution and the corner effect. The corner effect is used in this study to estimate the size of a concrete panel.

2. RESEARCH APPROACH

In this study, SAR imaging is used as a microwave sensor for characterizing the size (width) of concrete specimens. SAR imaging produces high-resolution coherent images with adjustable frequency bandwidth and radar aperture. Not only higher frequencies and wider bandwidths can lead to SAR images with better resolution, increased radar aperture due to prolonged radar movement can also produce high-resolution SAR images. Producing such coherent images from raw SAR data is an image formation algorithm. In SAR imaging, back-scattering pattern of any target is first formulated by a planar scattering problem in a domain Ω_s containing N scattering points. Consider an incident wave with unit amplitude as follows.[1]

Further author information: (Send correspondence to T. Yu)
E-mail: tzuyang_yu@UML.EDU, Telephone: 1 978 934 2288

Nondestructive Characterization and Monitoring of Advanced Materials, Aerospace, Civil Infrastructure, and Transportation XII, edited by Peter J. Shull, Andrew L. Gyekenyesi, Tzu-Yang Yu, H. Felix Wu, Proc. of SPIE Vol. 10599, 1059916 · © 2018 SPIE · CCC code: 0277-786X/18/$18 · doi: 10.1117/12.2294540

$$\psi_{inc}(\overline{r}) = \frac{1}{r}\exp(i\overline{k}_i.\overline{r}) \tag{1}$$

where $\overline{k}_i = k_{ix}\hat{x} - k_{ix}\hat{y}$ = the incident wave vector, and $\overline{r}$ = the position vector from the radar to any observation point; $|\overline{r}| = r$. The scattered field from scatterer j at $\overline{r}_j$ and observed at $\overline{r}$ is.[2]

$$\psi_{scat}(\overline{r}, \overline{r}_j) = \frac{s_j(\overline{r}, \hat{k}_i)}{|\overline{r} - \overline{r}_j|}\exp(ik|\overline{r} - \overline{r}_j|).\psi_{inc}(\overline{r}) \tag{2}$$

where $s_j = s_j(\overline{r}, \hat{k}_i)$ = the scattered amplitude at scatterer j due to an incident wave at $\hat{k}_i$ and observed at $\overline{r}$, $i = \sqrt{(-1)}$, $k = \frac{\omega}{c}$. Should we neglect the higher order interactions among scatterers in this formulation, the total scattered field from N scatterers observed at $\overline{r}$ is the summation of all the scattered fields as

$$\psi_{scat}(\overline{r}) = \sum_{j=1}^{N} \frac{s_j(\overline{r}, \hat{k}_i)}{|\overline{r} - \overline{r}_j|}\exp(ik|\overline{r} - \overline{r}_j|)\psi_{inc}(\overline{r}) \tag{3}$$

where $\overline{k}_s = k_{sx}\hat{x} + k_{sy}\hat{y}$ = the scattering direction vector, $\overline{k}_s = -\overline{k}_i$ when the radar operates in monostatic mode. Considering the case of a single scatterer without losing generality, Eq.(3) can be written as

$$\psi_{scat}(\omega, \theta) = \psi_{scat}(k, \overline{r}_s) = \frac{s_\theta}{r^2}\exp[i\frac{r}{c}\omega(1 + \cos^2\theta - \sin^2\theta)] \tag{4}$$

where $\theta = \theta_i = \tan^{-1}(\frac{k_{iy}}{k_{ix}})$. Eq.(4) is obtained by taking a slice of the two-dimensional (2D) Fourier transform (FT) of the domain Ω_s. In other reconstruction algorithms, all projections are superimposed before 2D IFT (plane projection) is carried out to obtain the final image. Therefore, the image plane $I(x, y) = I(r\cos\phi, r\sin\phi)$ can be reconstructed. Fig. (1) illustrates the processing step of the backprojection algorithm.[3]

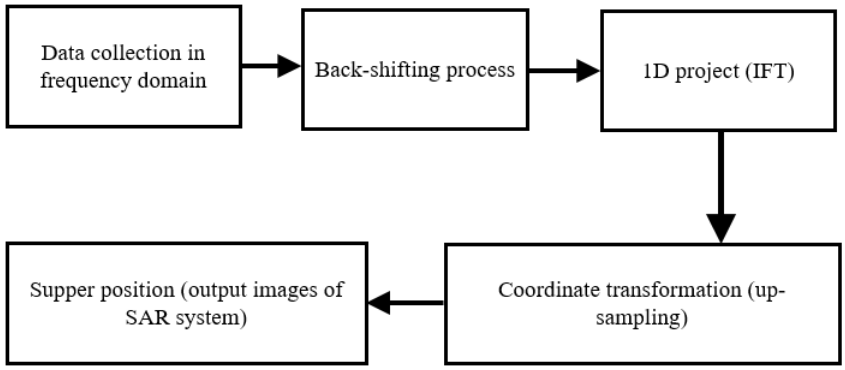

Figure 1. Backprojection algorithm processing steps

3. EXPERIMENTAL PROGRAM

3.1 Specimen Preparation

A 30cm-by-30cm-by-5cm concrete panel was designed and manufactured for the purpose of moisture characterization inside concrete. General purpose Type I/II Portland cement was used. The mix ratio (by weight) was 1:2:4 for cement: fine aggregate: coarse aggregate and the water-to-cement (w/c) ratio was 0.45. The concrete panel was moist cured for 28 days and stored in room condition (air-drying) for almost five months. Fig. 2 shows the schematic diagram and a picture of the concrete panel.

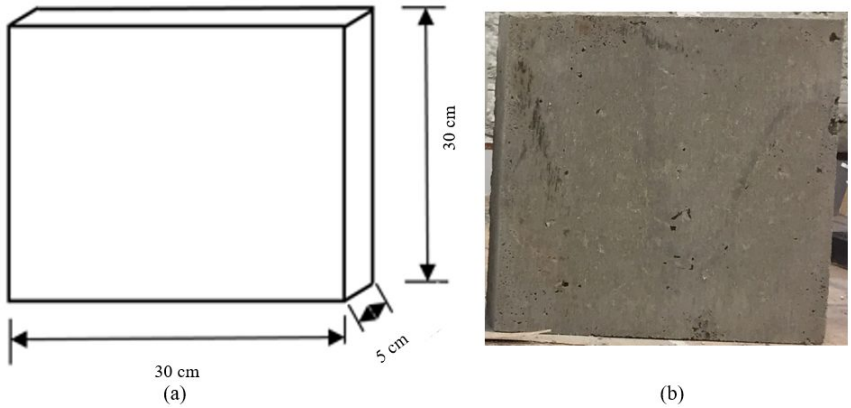

Figure 2. Schematic (a) and picture (b) of a concrete panel

3.2 Imaging Collection

Synthetic aperture radar (SAR) images of the concrete panel at various ranges were conducted using a 10 GHz continuous wave imaging radar (CWIR) system with a 1.5 GHz bandwidth inside an anechoic chamber in Electromagnetic Remote Sensing Laboratory at UMass Lowell. The CWIR system operates in the stripmap SAR mode by using a 2D positioner. The distance between the radar and the front surface of the concrete panel was denoted by $R = 15{\sim}200$ cm as shown in Fig. 3. The cross-range (r_x) distance of all SAR images was fixed to be 80 cm. Fig. 4 shows the schematic setup and a picture of the SAR imaging setup.

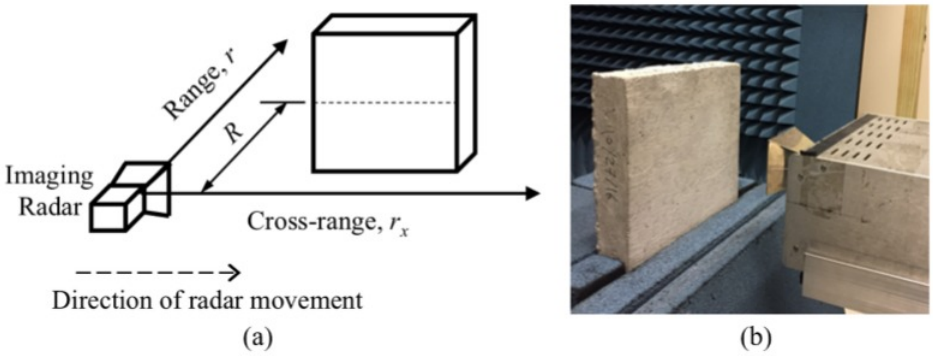

Figure 3. Schematics (a) and picture (b) of SAR imaging setup

4. RESULTS AND DISCUSSION

4.1 SAR Images at Different Ranges

As can be seen in Fig. 4, the maximum amplitude ($I_{\max}$) of a SAR image reduces when the range (R) of the image increases. Fig. 4 also shows that the corner scatterers of the SAR image of a concrete panel is affected by the range of the panel. The corner scatterers are formed when two surfaces have right angle facing the SAR imaging system, the reflection of singles twice off the surfaces and most of the radar energy is reflected back to the SAR imaging system. The corner scatterers get close to each other when the range increases until the maximum amplitude become singular scatterer as demonstrated in the $R = 200$ cm SAR image. This is because as the target gets faraway from the SAR system, two corner scatterers of the concrete panel merge into one. In other words, two corner scatterers of the concrete panel converge into singular scatterer in space when the range (R) becomes very large.

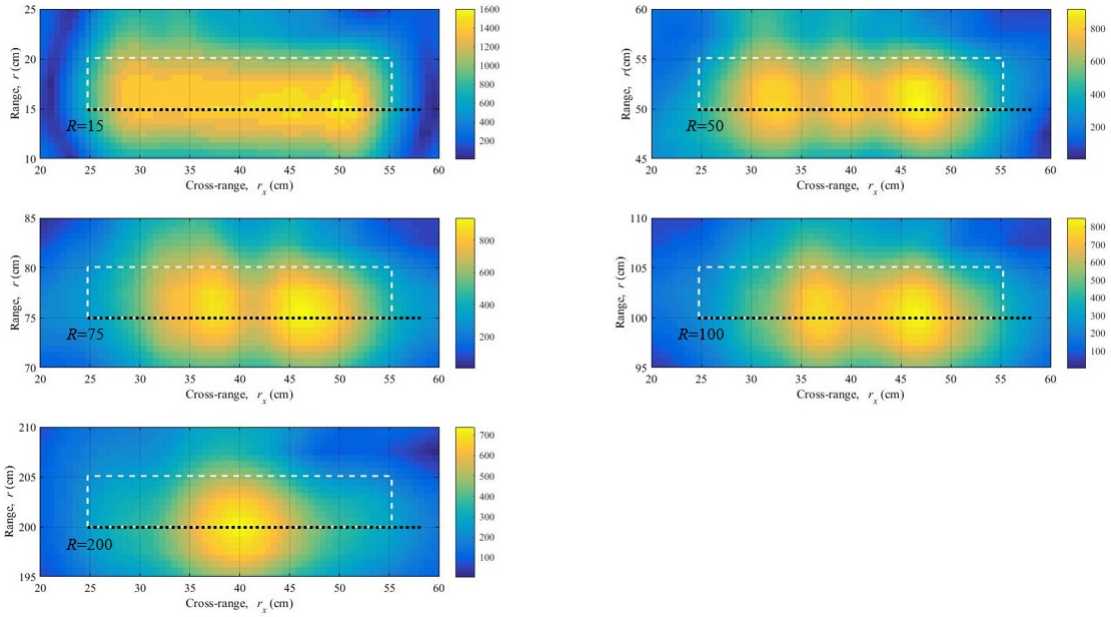

Figure 4. SAR images at different ranges (15cm, 50cm, 75cm, 100cm, 200cm)

4.2 Maximum SAR Amplitude at Various Ranges

Fig. 5 provides the quantitative comparison of SAR amplitudes of the concrete panel at various ranges, when only the SAR amplitudes on the front surface of the panel are considered. In Fig. 5, the ratio of maximum SAR amplitudes at ranges 200 cm and 15 cm was 0.45, while the ratio of maximum SAR amplitudes at ranges 75 cm and 15 cm was 0.568. It was found that the decrease of maximum SAR amplitudes at various ranges demonstrates a nonlinear pattern, as experimentally shown in Fig. 6 and modeled by Eq.(5). Eq.(5) represents an empirical model for estimating effective range of a concrete panel at ranges R = 15 cm$\sim$200 cm. This empirical model is associated with an error of 1% when compared with the actual ranges in our study.

$$r_{eff}(I_{\max}) = \left(\frac{I_{\max}}{2425}\right)^{-4.455} \tag{5}$$

where r_{eff} = effective range (cm) and $I_{\max}$ = maximum SAR amplitude. The coefficient of determination value of the Eq.(5) was 0.99. Comparison of Eq.(5) with other reported effective range estimation models provides a better understanding of Eq.(5). Fig. 6 illustrates the performance of Eq.(5). In Fig. 6, it is clear that a nonlinear relationship between effective range and maximum SAR amplitude exists. Eq.(6) is an effective range estimation model of a composite (brick-concrete) wall at ranges $R = 150 \sim 1500$ cm by using a 10 GHz imaging radar system.[4]

$$r_{eff}(I_{\max}) = \left(\frac{I_{\max}}{2234}\right)^{-3.7779} \tag{6}$$

It can be found that these effective range estimation models are different by their coefficients, indicating the difference in material property (concrete vs. composite) and geometry (panel vs. wall).

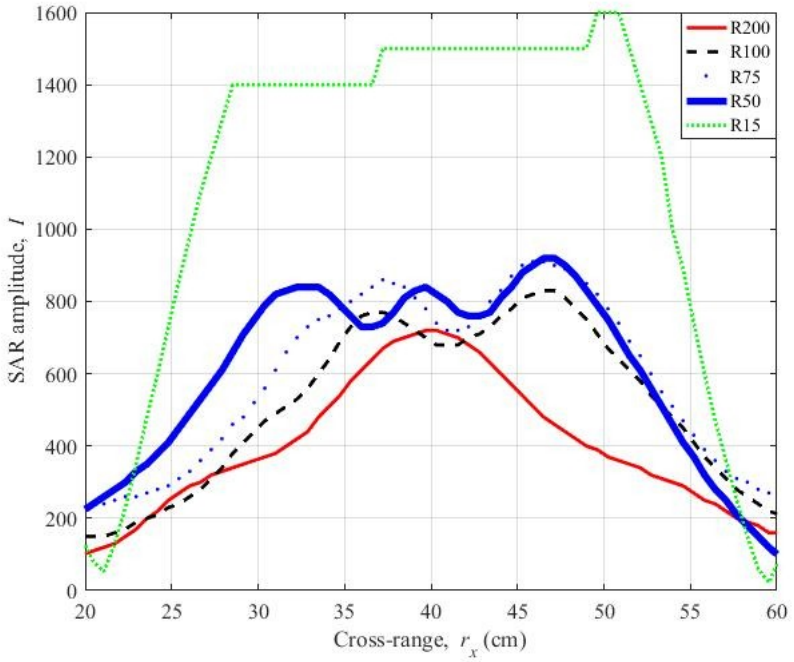

Figure 5. SAR curves at different ranges

4.3 Width Estimation

The width estimation approach of a concrete panel using SAR imaging is described in the following. Example calculation of width estimation at range ($R = 15$) is shown in Fig. 7. Observed from the SAR images in Fig. 4, the distance between the centers of two corner scatterers decreases with the increase of range R. Therefore, a cross-range parameter Δr_x was defined as shown in Fig. 8. Fig. 8 demonstrates the relationship of the variation of a cross-range parameter Δr_x along the range axis. This relationship was illustrated in Fig. 9 and modeled by Eq.(7).

$$\Delta r_x(r_{eff}) = -3.578{r_{eff}}^{0.4225} + 33.55 \tag{7}$$

where Δr_x = the distance between the centers of two corner scatterers (cm), and r_{eff} = effective range (cm). The coefficient of determination value of Eq.(7) was 0.98. Eq.(7) represents the empirical model for cross-range parameter Δr_x. Fig. 9 shows the performance of Eq.(7) for estimating cross-range parameter Δr_x. To predict the width of the concrete panel in this research, the cross-range parameter Δr_x was used in the following formulation. With Eq.(7), actual width (h) of the specimen was related to cross-range parameter Δr_x at effective range r_{eff} = 0 cm.

$$h(r_{eff}) = -3.578{r_{eff}}^{0.4225} + 33.55 + c' \tag{8}$$

Then c' = -3.07 cm. Substitute c' into Eq.(8) to arrive the inverse of Eq.(8) in Eq.(9).

$$h(\Delta r_x^m, r_{eff}) = \Delta r_x^m - 3.578{r_{eff}}^{0.4225} - 3.07 \tag{9}$$

where h = the width estimation of a concrete panel (cm), Δr_x^m = the measured cross-range distance between the centers of two corner scatterers. Eq.(9) represents the empirical model for width estimation of concrete panels in this research. Performance of Eq.(9) was found to be between 0.01% and 0.06% for SAR images from $R = 15$ cm to R =200 cm as can be seen in Fig. 10. Fig. 10 shows the raltionship between the width and the range of the concrete panel. The procedure of the width estimation of the concrete panel is shown in Fig. 11.

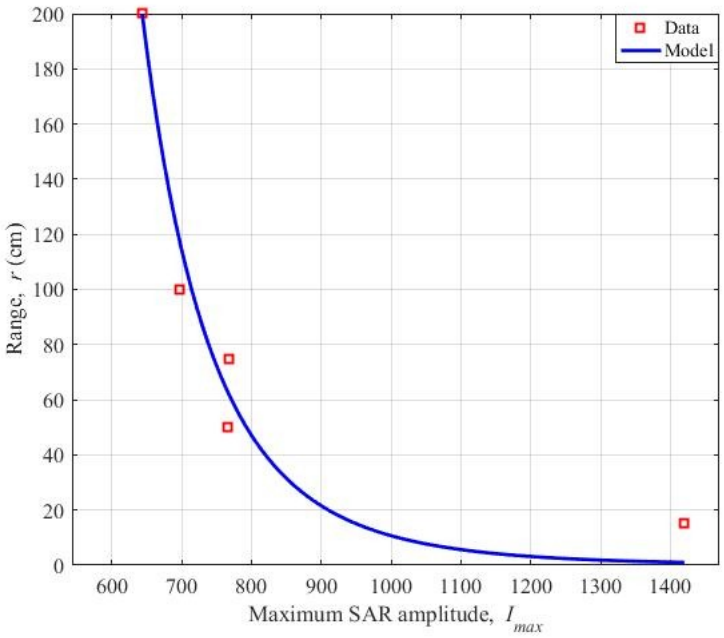

Figure 6. Maximum amplitude of SAR images at different ranges

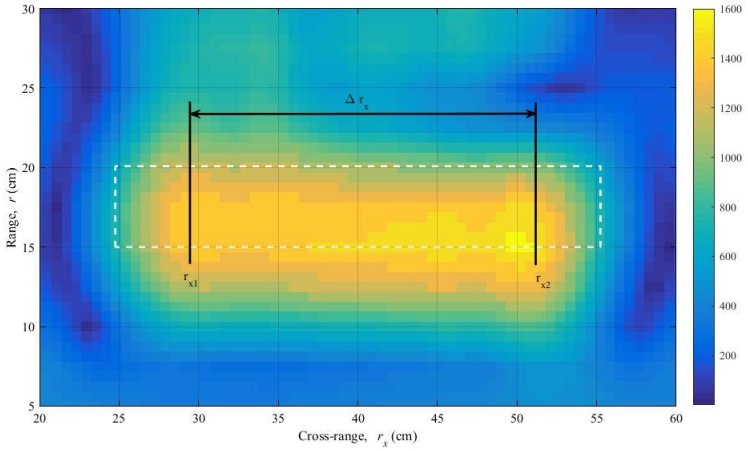

Figure 7. Example calculations of width estimation at $R = 15$ cm

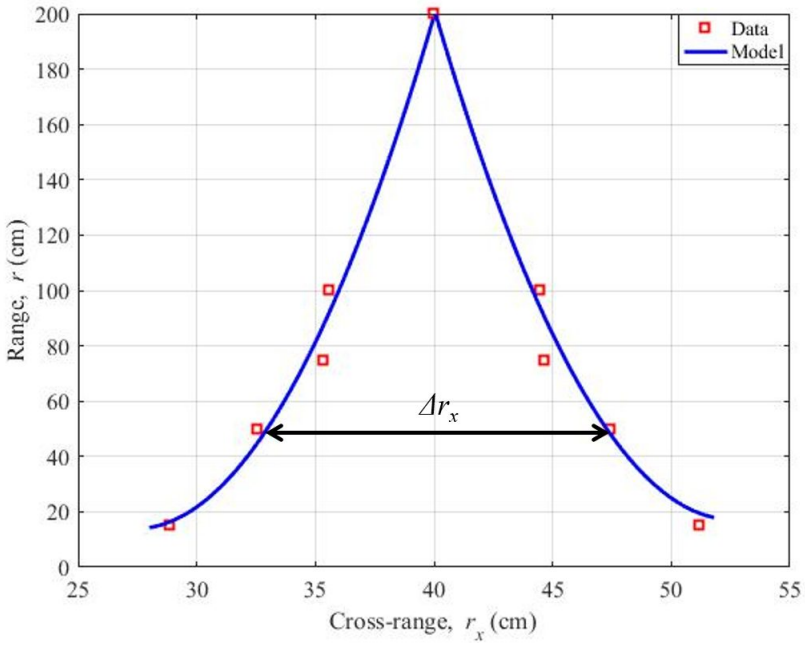

Figure 8. Variation of Δr_x along the range axis

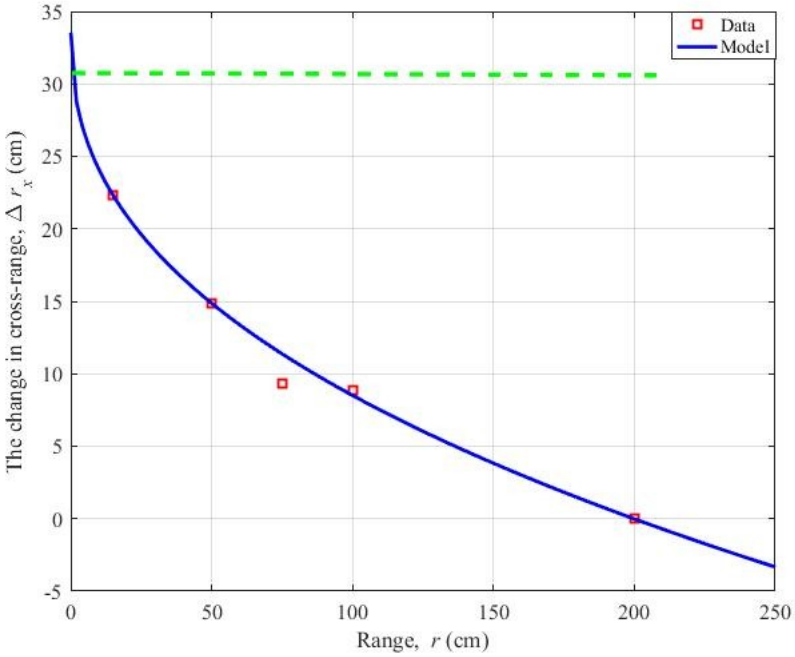

Figure 9. Distance between two corner scatterers in cross-range with varying ranges

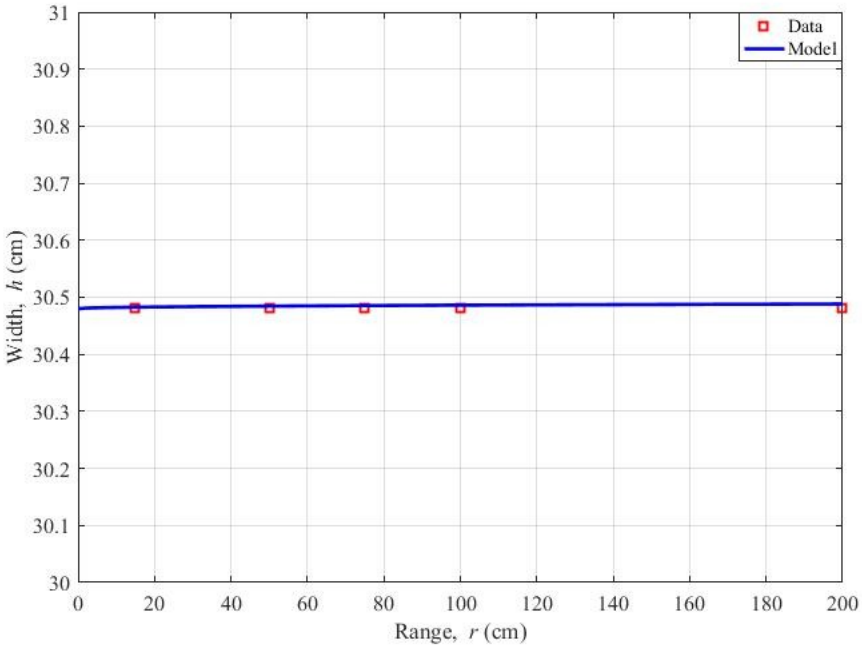

Figure 10. Performance of the model of a concrete panel

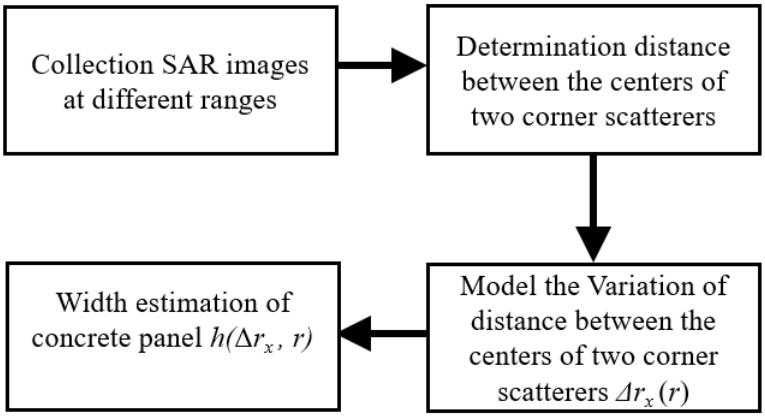

Figure 11. Procedure of width estimation

5. CONCLUSION

In this paper, the width estimation problem for concrete specimens using synthetic aperture radar (SAR) images was investigated. Size characterization of concrete specimens was experimentally studied by using a 10-GHz SAR imaging system inside an anechoic chamber at various ranges (15 cm, 50 cm 75 cm, 100 cm, and 200 cm). A 0.45 w/c ratio concrete panel was used in all SAR imaging experiments. It was found that the spatial feature of SAR images allows engineers to estimate the width of panel-like specimens at different ranges. Scattering response of specimen corners was imaged by circular scatterers in the range vs. cross-range (r, r_x) domain. It was demonstrated that, from our experimental study, the distance between the centers of two corner scatterers can be used to estimate the width of a concrete panel using SAR images. A four-step procedure was proposed, together with an empirical model, for using SAR images on width estimation. Attenuation of radar signals with the increase of range was also considered in this empirical model. It is believed that this approach can be applied to estimating other geometric features of concrete specimens of various shapes.

REFERENCES

[1] Kong, J., "Electromagnetic wave theory," EMW Publishing, Cambridge, MA (2000).

[2] Kong, J., Tsang, L., and Ding, K., "Scattering of electromagnetic waves, theories and applications," New York publishing: Wiley, Vol. 1 (2000).

[3] Yu, T.-Y., "Distant damage-assessment method for multilayer composite systems using electromagnetic waves," Journal of Engineering Mechanics 137(8), 547–560 (2011).

[4] Yu, T., Twumasi, J. O., Le, V., Tang, Q., and DAmico, N., "Surface and subsurface remote sensing of concrete structures using synthetic aperture radar imaging," Journal of Structural Engineering 143(10), 04017143 (2017).